Supporting Information

Fe/Fe_3C Particles Encapsulated in Hollow Carbon Nanoboxes for High Performance Zinc-Air Batteries

Chuyun Huang[a,b], Wenyuan Zhang[a], Xuezhi Hu[b], Shiliang Fei[b], Fhulufhelo Nemangwele[c], Nnditshedzeni Eric Maluta[c], Yangsen Hu[a], Hui Lv[a], Pei Hu[a] and Zhuo Peng[a]**

[a] China-South Africa PV-Hydrogen Energy Joint Research Center, School of Science, Hubei University of Technology (HBUT), Wuhan 430068, China.

[b] College of Mechanical and Electrical Engineering, Guangzhou City Construction College, Guangzhou 510900, China

[c] Department of Physics, University of Venda, Thohoyandou 0950, South Africa.

Methods and Materials

1 Materials

Zinc acetate dihydrate，trisodium citrate，tris (hydroxymethyl) aminomethane，potassium ferricyanide, hydrochloric acid and potassium hydroxide were purchased from China National Pharmaceutical Group Chemical Reagent Co., Ltd. Ammonium ferricyanide hydrate and dopamine hydrochloride was purchased from Aladdin Bio-Chem Technology Co., Ltd. Commercial platinum carbon was purchased from Johnson Matthey. Gas diffusion layers were purchased from Toray Industries, Japan. High-purity zinc sheets and nickel foam were purchased from Changsha Spring Industry Co., Ltd.

2 Preparation of Catalysts

The preparation of the catalyst is illustrated in Figure 1, beginning with the co-precipitation method to synthesize the Zn-Fe PBA precursor. This is followed by surface encapsulation using dopamine polymerization, and concluding with a thermal treatment to produce a hollow carbon-based catalyst. The detailed steps for each sample's preparation are as follows:

Zinc-Iron Prussian Blue Analog (Zn-Fe PBA): 0.177 g of zinc acetate dihydrate and 0.353 g of sodium citrate dihydrate are dissolved in 20 mL of ultrapure water to form Solution A. Separately, 0.126 g of ferrous cyanide hydrate is dispersed in 20 mL of ultrapure water to form Solution B. Solution B is then gradually added to Solution A with stirring for 30 minutes. After resting for 18 hours, the precipitate is collected

by centrifugation and dried at 60°C to obtain Zn-Fe PBA.

MOF materials, as precursors for synthesizing catalysts, allow for the adjustment of composition and geometric structure, enabling the customization of catalyst functions, thereby enhancing the catalytic activity of the catalyst.

Prussian Blue (PB): 7.6 g of polyvinylpyrrolidone (K30, PVP) and 0.22 g of potassium ferrocyanide are dissolved in 100 mL of 0.1 M hydrochloric acid. The mixture is stirred for 30 minutes and then heated to 80°C and maintained for 24 hours. The final product is obtained after centrifugation, washing, and drying to yield PB.

Encapsulated Dopamine-Coated Zinc-Iron Prussian Blue Analog or Prussian Blue (Zn-Fe PBA/PDA or PB/PDA): 0.1 g of Zn-Fe PBA or PB is ultrasonically dispersed in a 0.1 M tris(hydroxymethyl)aminomethane solution. Subsequently, 0.04 g of dopamine is added, and the mixture is stirred for 18 hours. After centrifugation and drying, Zn-Fe PBA/PDA or PB/PDA is obtained.

Encapsulation of Fe/Fe_3C Nanoparticles in Hollow Carbon Nano-Boxes (Fe/Fe_3C/HCNB), Carbon Nano-Boxes (Fe/Fe_3C/CNB), and Carbon Materials (Fe/Fe_3C/C): The magnetic boats loaded with Zn-Fe PBA/PDA, PB/PDA, or Zn-Fe PBA are placed in a tube furnace. Under an argon flow of 30 $mL \cdot min^{-1}$, the samples are heated to specific temperatures (600 to 900°C) to obtain Fe/Fe_3C/HCNB, Fe/Fe_3C/CNB, or Fe/Fe_3C/C. Note: Fe/Fe_3C/HCNB-T denotes the total assembly of Fe/Fe_3C/HCNB samples prepared at various temperatures, with a standard heating temperature of 700°C unless specified otherwise.

3 Physical Characterization of Samples

X-ray diffraction (XRD) is a technique where X-rays are directed at crystalline materials, producing reflected signals with a path difference between two atomic layers of a crystal plane. Diffraction occurs when this path difference equals an integer multiple of the interplanar spacing, allowing identification of specific crystal planes through characteristic diffraction peaks. Comparative analysis with standard diffraction patterns from PDF cards enables material characterization. For this study, the X'Pert PRO model XRD powder diffractometer was used, operating over a scan range of 15–75° at a speed of 8° per minute. Scanning Electron Microscopy (SEM) involves bombarding the sample surface with accelerated electrons and collecting the reflected secondary electrons to analyze the sample's morphology. The SEM used in this study is the FEI Nova NanoSEM 450, with an acceleration voltage of 10 kV and a beam spot size of 3. Transmission Electron Microscopy (TEM) employs a high-voltage accelerated and focused electron beam projected onto the sample. The instrument captures electrons transmitted through the sample, creating images that reveal microscopic morphologies. High-energy electron beams can also excite inner-shell electrons of sample atoms, causing vacancies followed by spontaneous electron transitions that generate X-ray fluorescence, enabling elemental analysis via fluorescence spectroscopy. The TEM model used here is the FEI Tecnai G2 F30, operated at 200 kV for standard TEM images, dark-field scanning transmission electron microscopy (STEM), and high-resolution transmission electron microscopy (HRTEM) images. Energy-dispersive spectroscopy was performed at 300 kV. X-ray

Photoelectron Spectroscopy (XPS) involves irradiating the solid surface with X-rays to excite surface atoms to emit photoelectrons, which are then captured and analyzed by an energy analyzer to determine the elemental composition and valence states of the sample surface. The experiments were conducted using the Shimadzu AXIS-ULTRA DLD-600W X-ray photoelectron spectrometer, calibrated using the C1s peak at 285.0 eV. Raman spectroscopy is based on the Raman scattering effect, where incident light of a specific frequency scatters off a sample, changing frequency. Analyzing these scattered light frequencies different from the incident light provides information on the vibrational and rotational aspects of sample molecules. The LabRam HR800 Raman spectrometer was used in this study, employing a 532 nm excitation source. The surface area of the sample was determined by measuring nitrogen adsorption-desorption isotherms at low temperatures (77 K) and analyzing them using the Barrett-Joyner-Halenda (BJH) method. The ASAP2420-4MP fully automatic surface area analyzer was utilized for this testing. Prior to contact angle testing, the sample was coated on the surface of an air electrode, and specific alkaline droplets were used for the contact angle tests. The instrument used was the HCJ-BH contact angle meter produced by Beijing Jingcheng Huatai Instrument Co., Ltd. Inductively Coupled Plasma Atomic Emission Spectroscopy (ICP-AES) uses an inductively coupled plasma as an excitation source. It analyzes the specific signals emitted by ions as they return to their ground state to determine the types and concentrations of elements. The elemental analysis was performed using the Thermo Elemental IRIS Advantage spectrometer. metal cation content (mole ratio) was

determined by inductively coupled plasma (ICP, Leeman Labs, Prodigy Plus).

4 Electrochemical Performance Testing

Electrochemical tests were conducted at the Wuhan Costech CS350 electrochemical workstation using a traditional three-electrode system. A 5 mm diameter glassy carbon electrode equipped with a Pine rotating disk electrode apparatus served as the working electrode. A platinum sheet (1*1 cm^2) was used as the counter electrode, and a saturated calomel electrode (SCE) with a salt bridge functioned as the reference electrode. Unless specifically noted, all potentials provided herein are relative to the reversible hydrogen electrode (RHE), with the electrode potential conversion formula shown as equation 1:

$$E_{RHE} = E_{SCE} + 0.059 \times pH + E_{SCE}^{0} \quad \left(E_{SCE}^{0} = 0.242\ V\right) \qquad (1)$$

Preparation of the Working Electrode:5 mg of the sample was ultrasonically dispersed in 1 mL of 0.1 wt.% Nafion ethanol solution to form an ink dispersion. 14 μL of this dispersion was pipetted onto the surface of the glassy carbon electrode (loading: 0.357 $mg \cdot cm^2$) and dried before testing.

Oxygen Reduction Reaction (ORR) Test:The electrochemical window for cyclic voltammetry (CV) tests was 0 to 1.2 V, conducted in deoxygenated and oxygen-saturated 0.1 M KOH solution, with a scan rate of 50 $mV \cdot s^{-1}$. Linear sweep voltammetry (LSV) tests at different rotation speeds also used an electrochemical window of 0 to 1.2 V, with a scan rate of 5 $mV \cdot s^{-1}$. The electrochemical stability of the catalyst was assessed by comparing the overlap of CV and LSV curves before and

after 3000 CV cycles.

Calculation of ORR Electron Transfer Number (n) and Kinetic Current Density (JK) can be done using the Koutecky-Levich (K-L) equations 2 to 4:

$$J^{-1} = J_L^{-1} + J_K^{-1} = B^{-1}\omega^{-\frac{1}{2}} + J_K^{-1} \quad (2)$$

$$B = 0.2nFC_0 D_0^{\frac{2}{3}} v^{-\frac{1}{6}} \quad (3)$$

$$J_K = nFkC_0 \quad (4)$$

Here, J and J_L represent the test current density and the limiting diffusion current density, respectively, ω is the rotation speed of the disk (rpm), F is the Faraday constant (96485), $C_0$is the volumetric concentration of oxygen ($1.21*10^{-6}$ mol·cm^{-3}), D_0 is the diffusion rate of oxygen ($1.9*10^{-5}$ cm^2·s^{-1}), and v is the viscosity of the electrolyte (0.01 cm^2·s^{-1}).

According to the RRDE results, the peroxide species yield (HO_2^-%) and the electron transfer number (n) were calculated with the following equations:

$$n = \frac{4|i_d|}{|i_d| + i_r/N}$$

$$HO_2^-(\%) = \frac{2i_r/N}{|i_d| + i_r/N} \times 100\%$$

Where i_d is disk current, i_r is ring current, and N represents current collection efficiency of the Pt ring (0.37).

5 Assembly and Testing of a Primary Zinc-Air Battery

In the assembly of a primary zinc-air battery, the ink dispersion prepared in the previous section is uniformly applied to the gas diffusion layer to serve as the air electrode, with a loading of 0.5 $mg \cdot cm^{-2}$. High-purity zinc sheets (99.999%) are used as the anode, while the electrolyte consists of a 6 M KOH solution containing 0.2 M zinc acetate. The discharge curves are evaluated through Linear Sweep Voltammetry (LSV) tests within a voltage window of 1.4 to 0.3 V. The battery's discharge stability is assessed via constant current polarization, with the stability determined by the potential-time decay curves. The capacity density of the battery is calculated based on the mass change of the zinc electrode before and after the constant current tests. The rate capability of the battery is determined through a series of constant current discharge tests at varying current densities.

Additionally, this study employs a mercury/mercuric oxide (Hg/HgO) electrode as the reference electrode and a platinum wire as the counter electrode to perform three-electrode electrochemical testing on the air electrode. The electrochemical window for the LSV tests ranges from 0 V to -1 V (relative to the Hg/HgO electrode), with a scan rate of 5 $mV \cdot s^{-1}$. Electrochemical Impedance Spectroscopy (EIS) tests are conducted at various biases within a frequency range of 100 kHz to 0.01 Hz, with an AC amplitude of 5 mV.

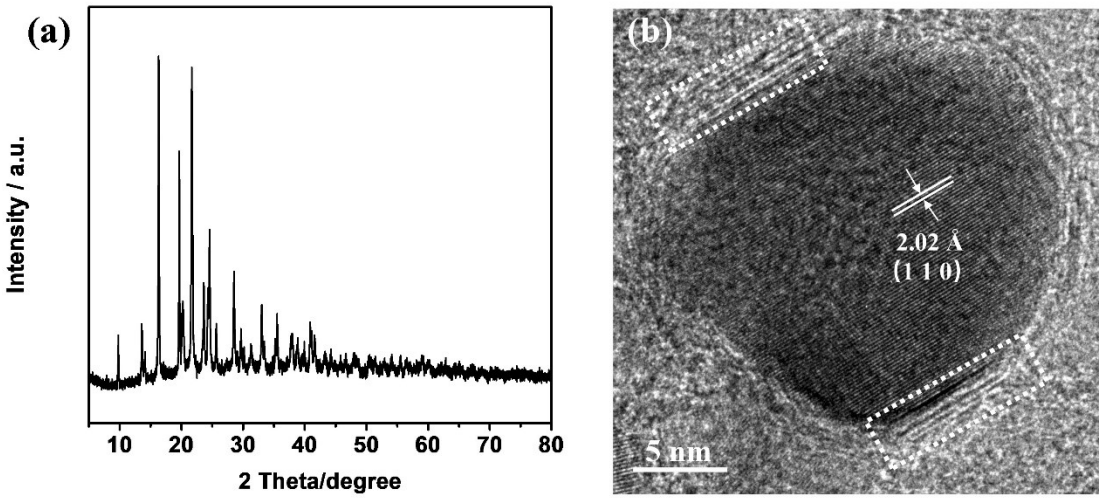

Figure S1 XRD pattern of Zn-Fe PBA (a). HRTEM image of Fe/Fe_3C/HCNB (b).

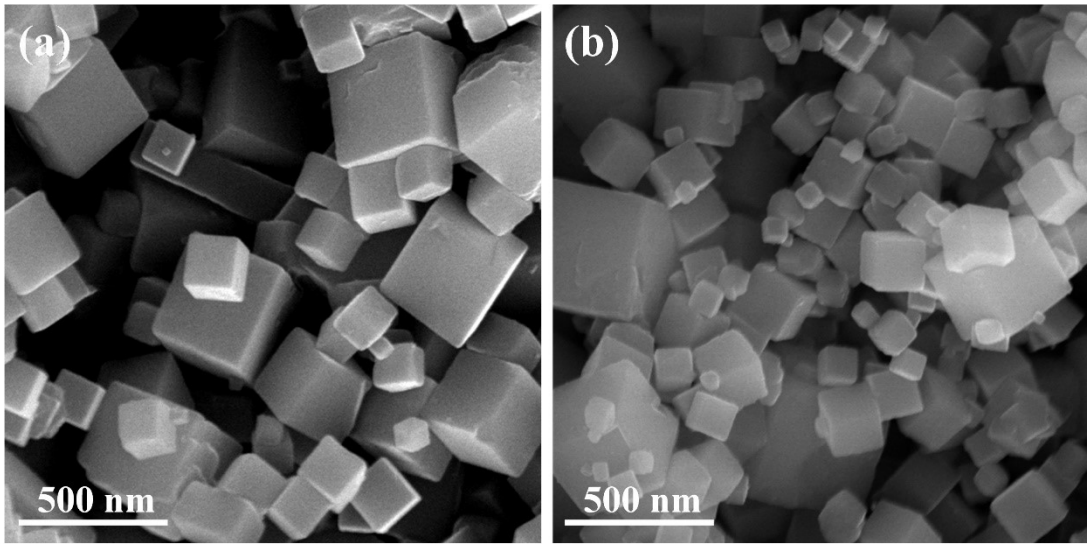

Figure S2 SEM images of PB (a) and PB/PDA (b), respectively.

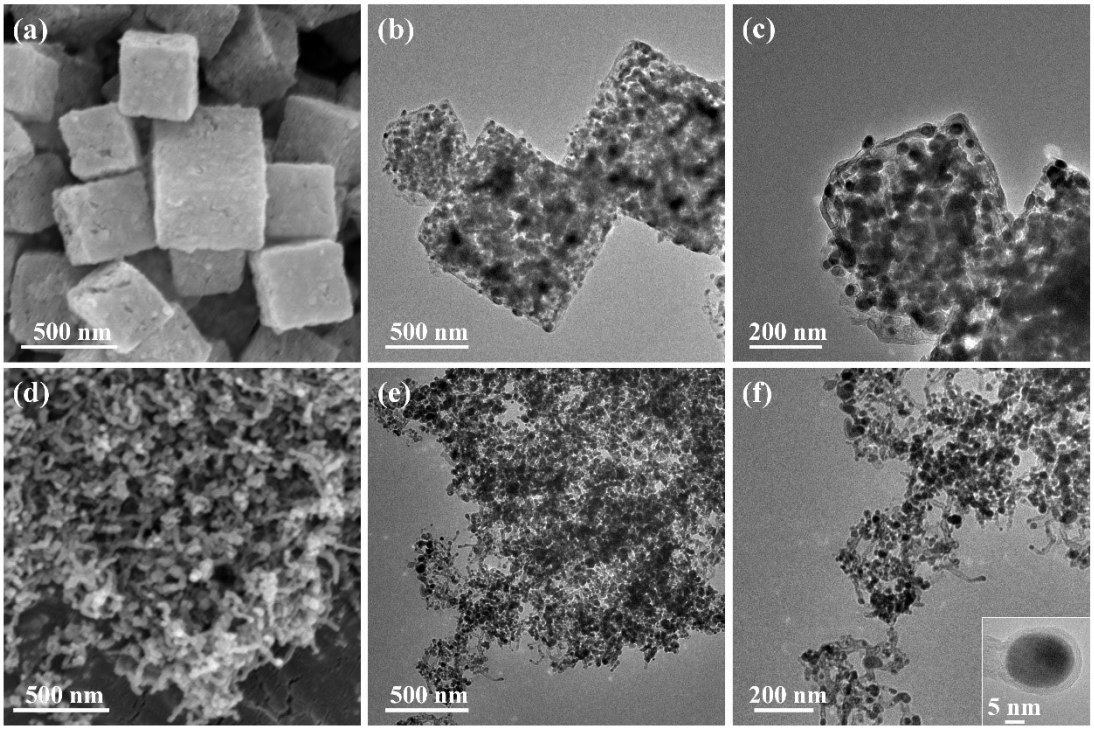

Figure S3 SEM (a) and TEM (b-c) images of $Fe/Fe_3C/CNB$. SEM (d) and TEM (e-f) images of $Fe/Fe_3C/C$.

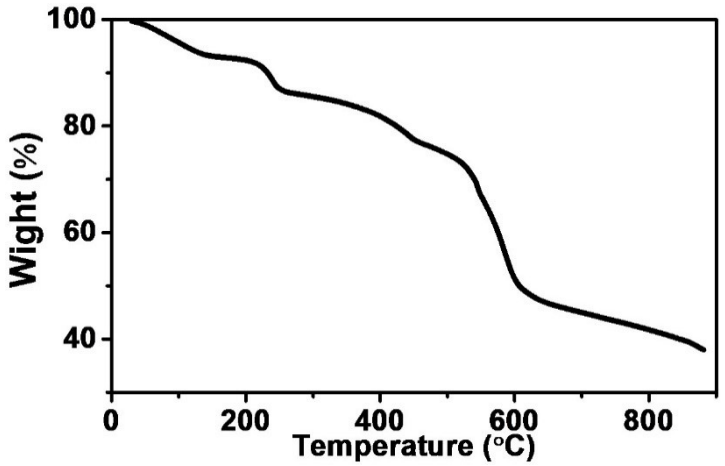

Figure S4 TGA curve of Zn-Fe PBA/PDA in N_2 atmosphere.

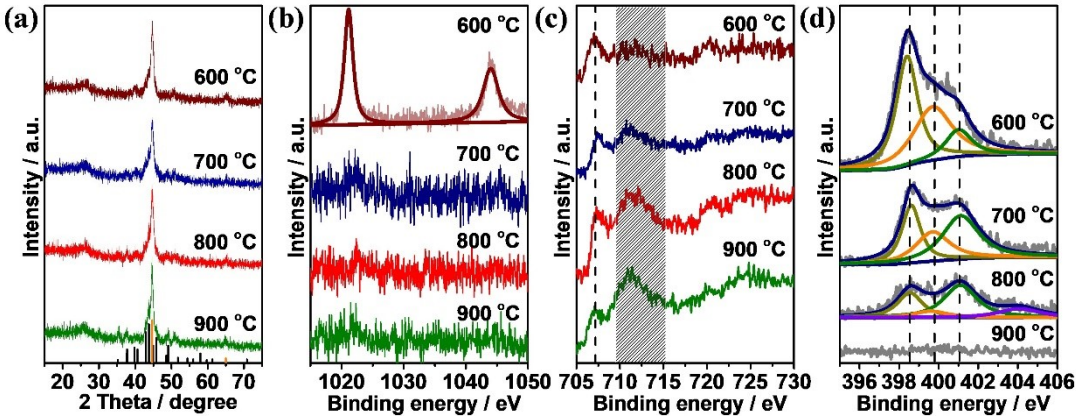

Figure S5 XRD patterns (a) of Fe/Fe_3C/HCNB-T. Zn 2p (b), Fe 2p (c) and N 1s (d) highresolution XPS spectra of Fe/Fe_3C/HCNB-T.

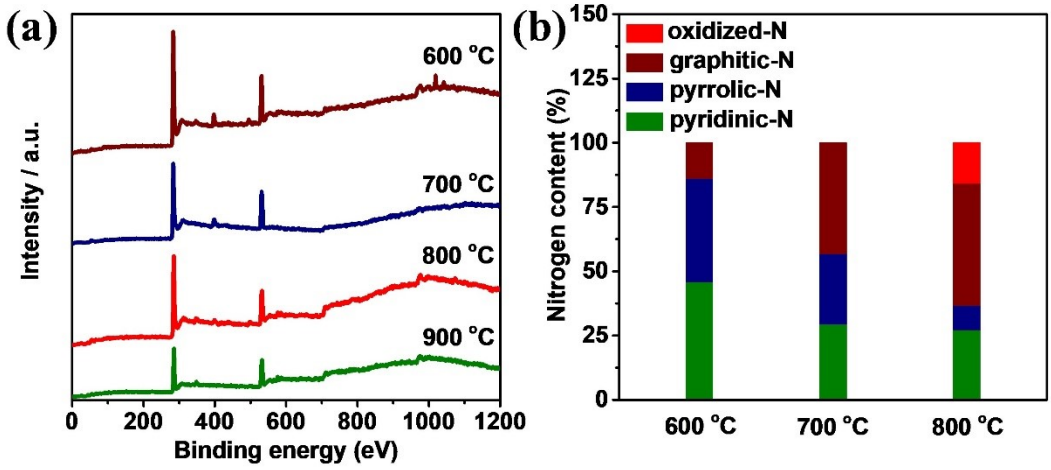

Figure S6 Survey XPS spectra of Fe/Fe_3C/HCNB-T (a). Nitrogen content of Fe/Fe_3C/HCNB-T(b)

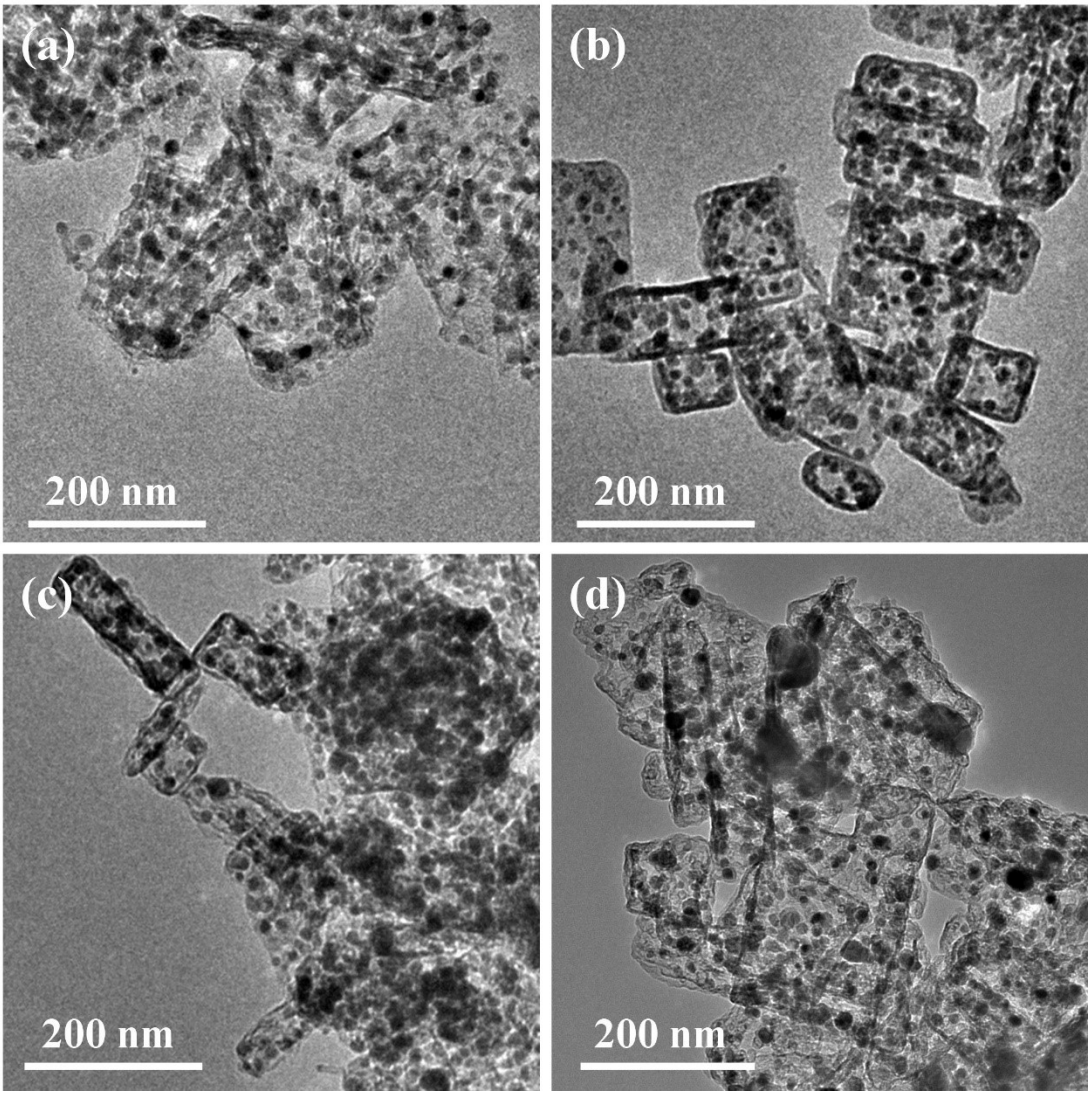

Figure S7 TEM images of $Fe/Fe_3C/HCNB$-600 (a), $Fe/Fe_3C/HCNB$-700 (b), $Fe/Fe_3C/HCNB$.800(c)and $Fe/Fe_3C/HCNB$-900(d).

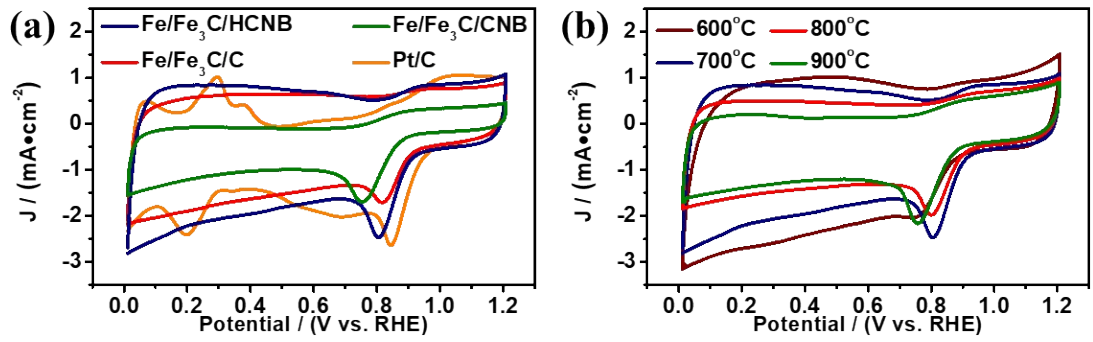

Figure S8 CV curves of varies samples in O_2 saturated 0.1 M KOH solution

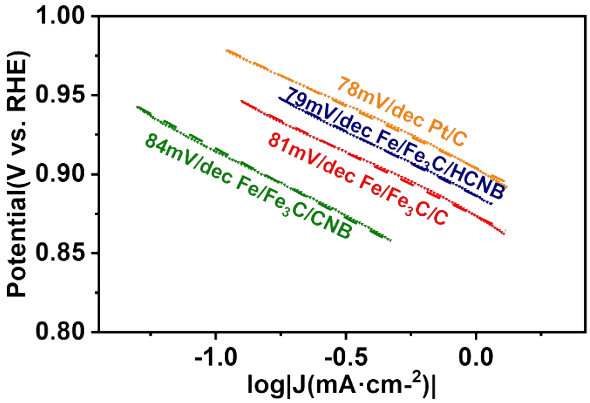

Figure S9. Tafel slopes of Pt/C, Fe/Fe_3C/C, Fe/Fe_3C/CNB and Fe/Fe_3C/HCNB in O_2-saturated 0.1 M KOH solution at 1600 rpm.

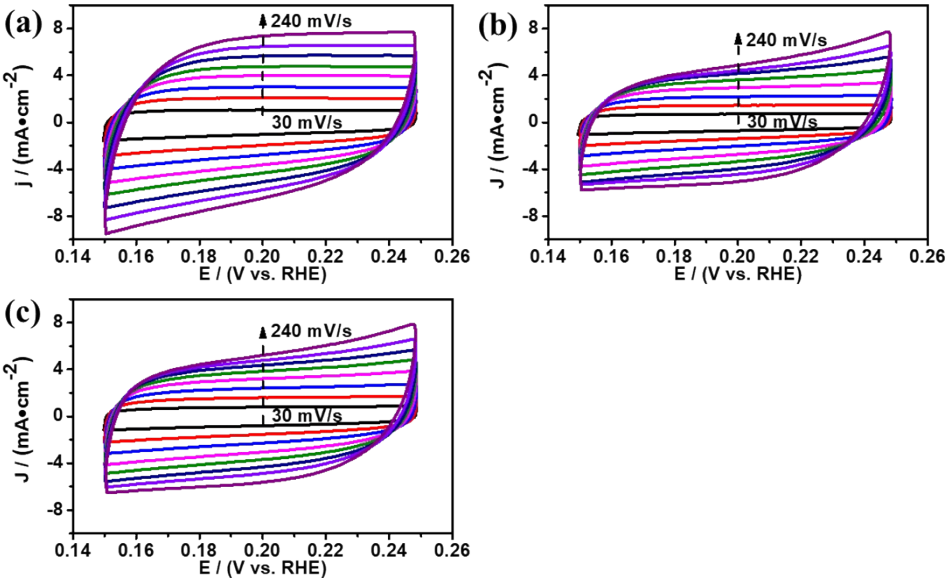

Figure S10. CV curves of (a) Fe/Fe_3C/HCNB, (b) Fe/Fe_3C/CNB, and (c) Fe/Fe_3C/C modified electrodes in the double layer region at scan rates of 30-240 mV s^{-1} in 1.0 M KOH solution

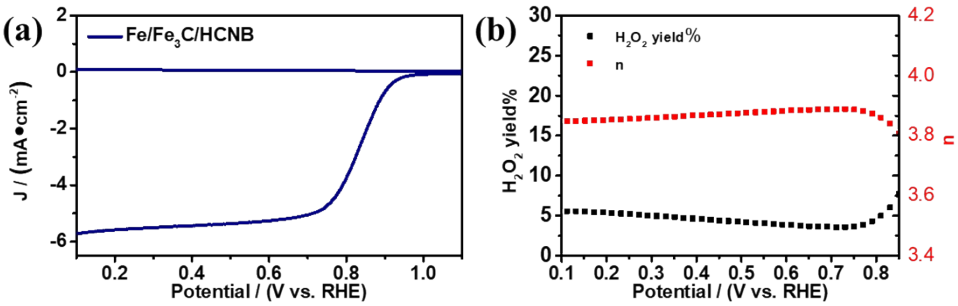

Figure S11 RRDE test, HO_2^- and calculated electron transfer number of Fe/Fe_3C/HCNB

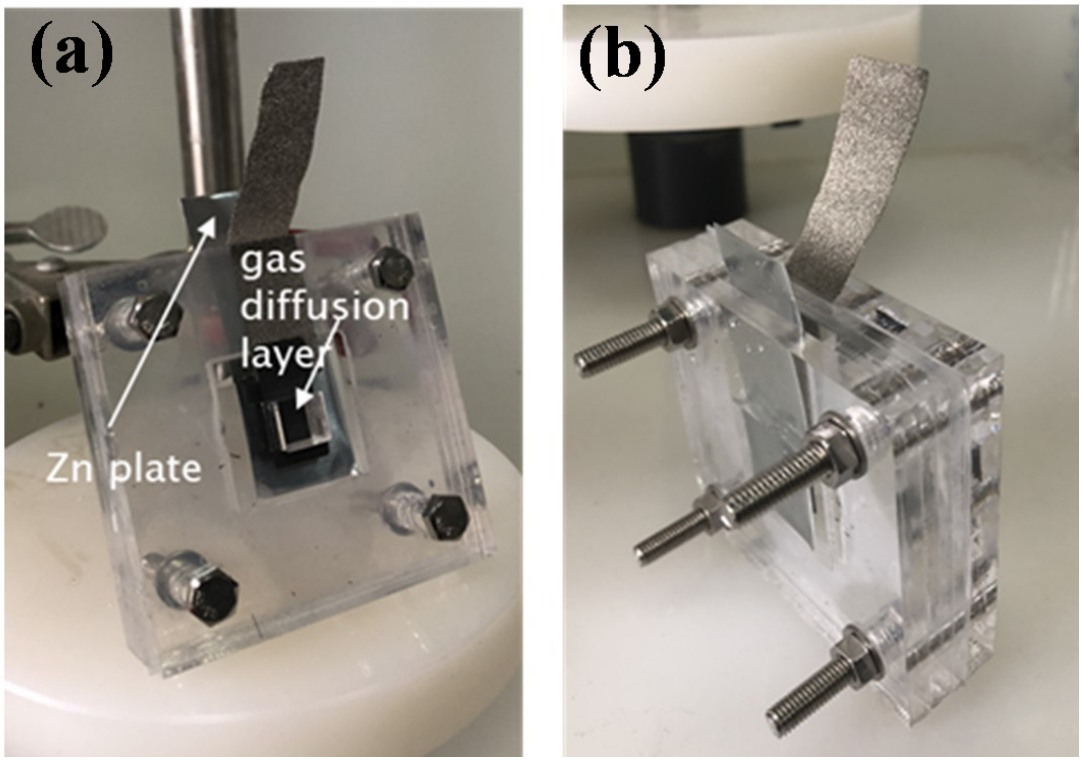

Figure S12 Front (a) and back (b) optical images of home-made Zn-air battery device.

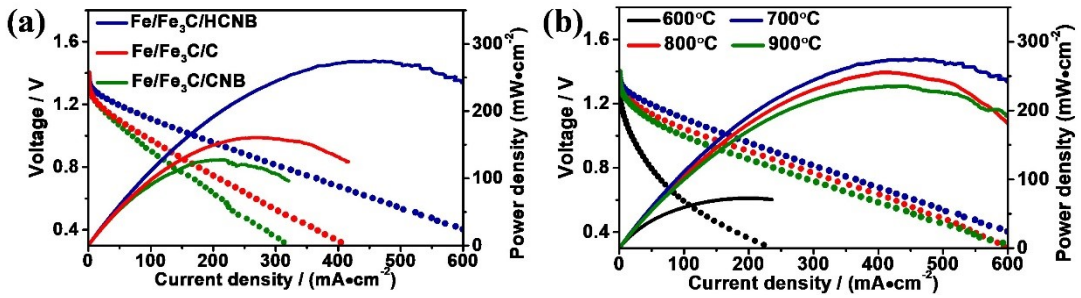

Figure S13 Discharge polarization curves and corresponding power density curves of Fe/Fe_3C/HCNB, Fe/Fe_3C/CNB and Fe/Fe_3C/C based battery (a). Discharge polarization curves and corresponding power density curves of Fe/Fe_3C/HCNB-T based battery (b).

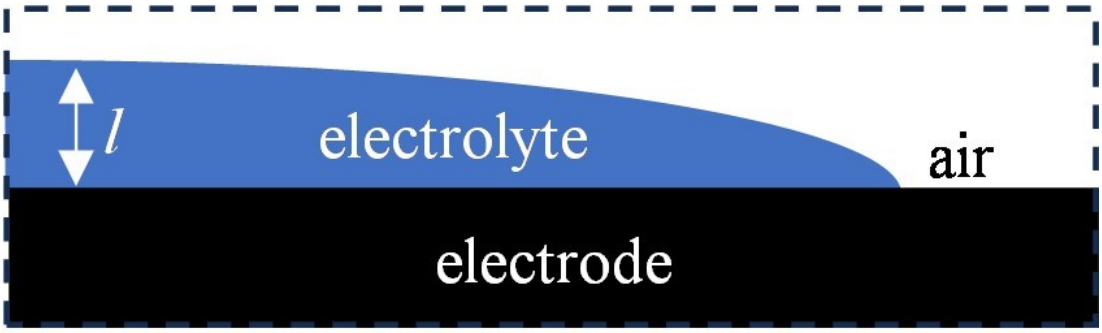

Figure S14 Illustration of solid-liquid-gas three phases junction on gas diffusion layer.

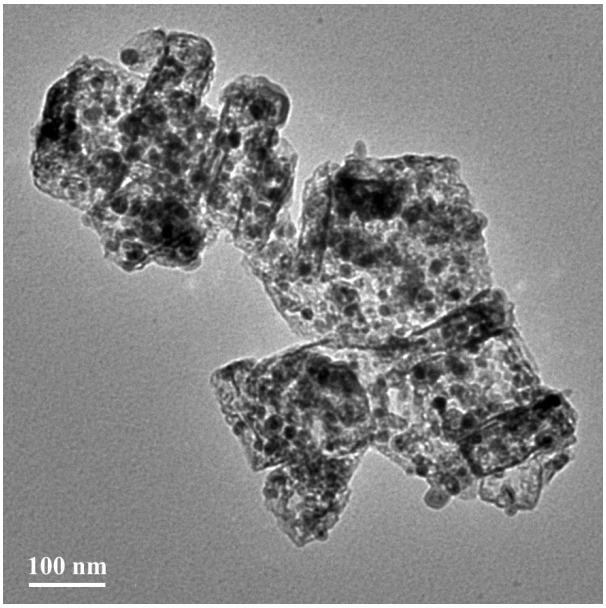

Figure S15 TEM image of Fe/Fe_3C/HCNB after constant current discharge of 100 mA·cm^{-2} for 2 hours.

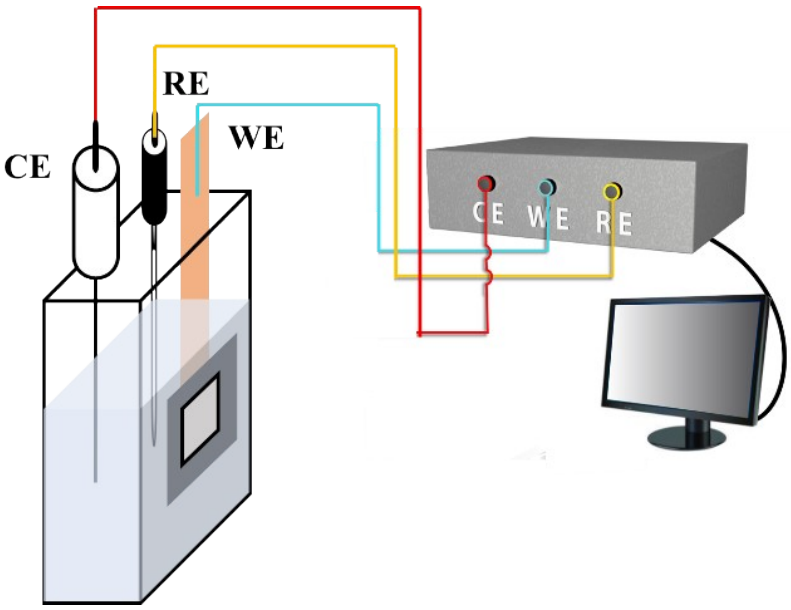

Figure S16 Illustration of home-made three-electrode system using gas diffusion electrode asworking electrode.

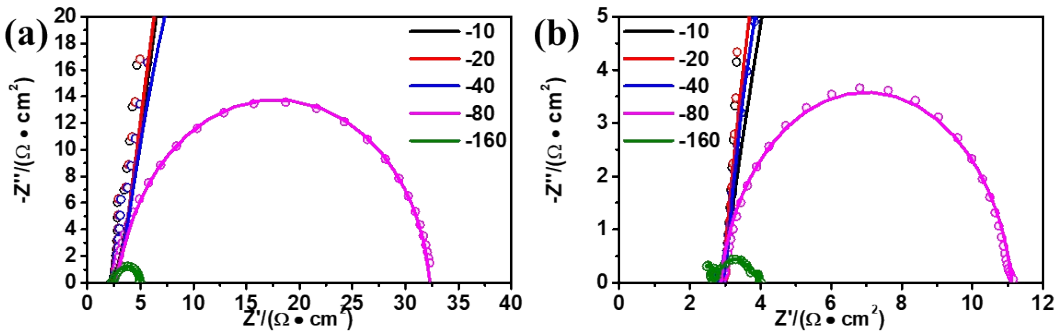

Figure S17 Amplification diagram under high overpotential of EIS test.

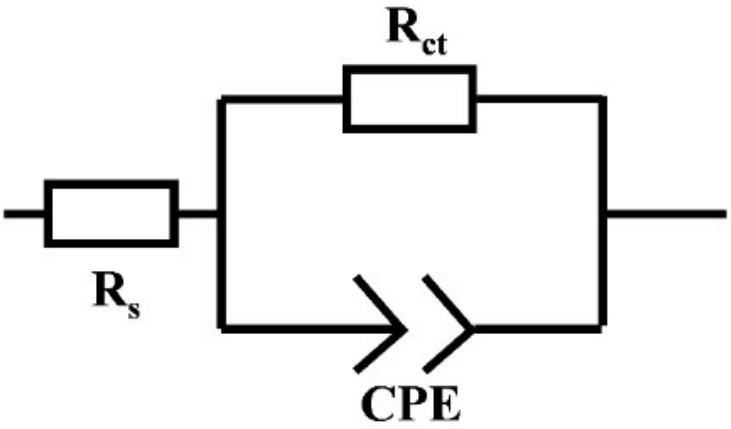

Figure S18 Equivalent circuit for fitting EIS data (Rs is solution resistance, Rct and CPE arecharge transfer resistance and double layer between solution and electrode, respectively).

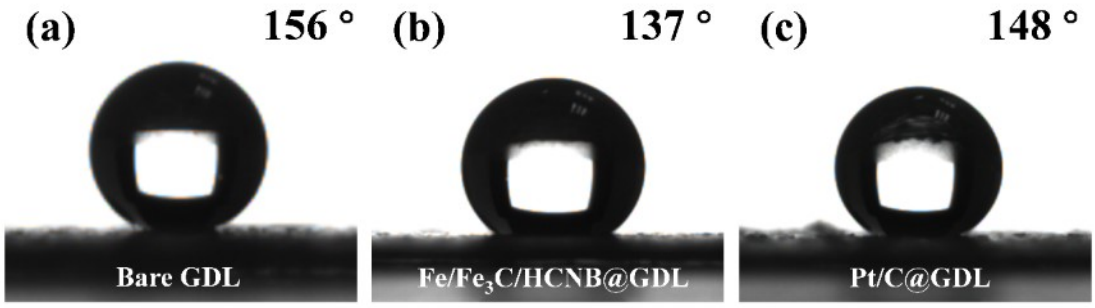

Figure S19 Contact angle tests of Bare GDL (a), Fe/Fe3C/HCNB coated GDL (b) and Pt/C coatedGDL (c).

Table S1 Metal element content (wt%) of Fe/Fe_3C/HCNB-T from ICP data

	Fe	Zn
Fe/Fe_3C/HCNB-600	8.67	8.66
Fe/Fe_3C/HCNB-700	10.68	3.57
Fe/Fe_3C/HCNB-800	11.54	2.84
Fe/Fe_3C/HCNB-900	20.95	0.93

Table S2. Chose some performances of recent reported electrocatalysts and compared with our work

Materials	Half-wave potential	limiting current density	Ref
NiCo-NG	0.793	7.64	*Microporous Mesoporous Mater*, 2024, **380**, 113292.
FeS-NS-CNT-900	0.877	-	*J ALLOY COMPD*, 2024, **1008**, 176525
Co/Fe/Ni M-N-C	0.87	5.68	*J. Energy Storage*, 2024, **101**, 113772
G/Co-N-C-0.025	0.87	4.6	*J. Power Sources*, 2024, **615**, 235103
F-S-N-C	0.808	-	*Int. J. Hydrogen Energy*, 2024, **83**, 1107-1112
Co-N-CNT-800	0.89	5.1	*Solid State Sci*, 2024, **154**, 107623

$LaMn_2O_5$@GO	0.82	-	*Solid State Sci*, 2024, **154**, 107623
NiO/IrO_2- NF	0.8	-	*APPL CATAL B-ENVIRON*, 2024, **355**, 124196
Ni_1Co_3-LDH/GNF	0.79	-	*J. Energy Storage*, 2024, **90**, 111845
Co/CoO_x–N–C	0.83	5.85	*Chem. Eng. J*, 2024, **498**, 155822
FeZn-NC	0.9	5.15	*J. Electroanal. Chem*, 2024, **967**, 118475
FeNi-NC	0.852	-	*Chem. Eng. J*, 2024, **497**, 154963.
$NiFe_2O_4$/TiO_2@ Ti_3C_2–2	0.846		*J. Energy Storage*, 2024, **98**, 113139
$MnCo_2O_4$-6	0.64	5.49	*Vacuum*, 2024, **227**, 113416
Zr_2ON_2@NiFe LDH	0.66	-	*J COLLOID INTERF SCI*, 2024, **672**, 610-617.
This article	0.826	5.8	

Table S3. Summary of various bifunctional electrocatalysts for liquid Zn-air battery.

Materials	Power Density	Specific Capacity	Ref
PAMNa-CMCS$_x$/Ele	120.87	704.34	*Chem. Eng. J*, 2023, **468**, 143836.
FeNSPC	91	702	*J. Energy Storage*, 2023, **70**, 107950.
M-Fe_2O_3/FeSA@NC	155	762	*J. Energy Chem*, 2023, **85**, 154-163
Selenium-doped CoS_2	156.24	620.67	*APPL CATAL B-ENVIRON*, 2023, **330**, 122523.
FeNi LDH	118	798	*Adv. Mater*, 2023, **35**, 2210550.
CoCu/N-CNS	104.3	771.7	*Small*, 2023, **19**, 2207413.
FePc@NC-1000	120.37	725	*J COLLOID INTERF SCI*, 2023, **650**, 2056-2064.
FeNi@NC-900	119	830.1	*J COLLOID INTERF SCI*, 2023, **641**, 265-276
F-$FeWO_4$/NC	173.5	800.2	*Mater. Today Phys*, 2023, **38**, 101274

CoP/HNBs@NCL	139.8	728.8	*Chem. Eng. J,* 2023, **475**, 146154
Fe_3O_4/CoO@CF	137	740	*J COLLOID INTERF SCI*, 2023, **640**, 549-557
$Ni/Ni_{12}P_5$@CNx	181	710	*J COLLOID INTERF SCI*, 2023, **642**, 439-446
$Fe_{1.2}(CoNi)_{1.8}S_6$MES	124	808	*APPL CATAL B-ENVIRON*, 2023, **325**, 122356
AlF_3@HPCNFs-3	181	796	*J COLLOID INTERF SCI*, 2024, **654**, 1063-1079
VN-MgO	165	661	*APPL CATAL B-ENVIRON*, 2023, **335**, 122895
FeNi NHC	126	785.3	*Nano Energy*, 2023, **118**, 108952
CoP/HNBs@NCL-2	139.8	728.8	*Chem. Eng. J*, 2023, **475**, 146154
N/P-C-CoP-850	151	773.8	*Chem. Eng. J*, 2022, **428**, 131225
Co2P@NPPC	226	797	*Catal. Sci. Technol*, 2023, **13**, 3084-3093
Bi–CoP/NP-DG	122	752	*J. Mater. Chem. A*, 2019, **7**, 22507-22513
This article	276	796	